Research Article

High-temperature oxidation kinetics of Cu bearing carbon steel

Selçuk Yeşiltepe[1] · Mustafa Kelami Şeşen[1]

Received: 29 January 2020 / Accepted: 10 March 2020 / Published online: 13 March 2020

Abstract
In this article, oxidation kinetics of carbon steel is investigated with respect to the existence of copper (Cu). It is aimed to figure out the high-temperature oxidation behaviours of Cu bearing steel. Cu induced hot shortness is the main problem of recycling of tramp element containing steels. The experimental temperature range was decided according to the steel deformation process'. Oxidation experiments were conducted between 900 and 1200 °C with 100 °C intervals in an electrical resistance furnace. High-temperature oxidation kinetics of Cu bearing carbon steel was examined. Topographical surface analysis' of samples were carried out via X-ray diffraction, scanning electron microscopy, optical microscopy. Mass gain rate and kinetical results were algebraically evaluated. Cu segregation on steel surface at elevated temperatures and its behaviour against oxygen were observed.

Keywords Copper enrichment · Oxidation kinetics · Tramp element · Scale · Steel

1 Introduction

Oxidation kinetics of materials is highly studied for different materials under various conditions. High-temperature oxidation is affected by atmospheric conditions, the partial pressure of gases, temperature, material conditions such as surface roughness, alloying, and coating, etcetera. Tramp element behaviours in steels are crucial to understanding because the recycling of steel increases tramp element concentration in scrap continuously. Cu is not able to be refined from steel via conventional steelmaking in electric arc furnace (EAF) due to the nature of the process. The conventional EAF process follows the oxidation route for impurities with basic oxide slags. Cu, arsenic, antimony, and tin cannot be refined via the EAF process, and in every recycling step, these elements accumulate in the steel. Accumulated elements are called as tramp elements in steel [1–6].

Tramp element behaviours in steels are known as hazardous effects. Cu has the highest concentration as a tramp element in steel scraps. The solution of Cu-induced problems in carbon steel at industrial practice is based on using cleaner scrap or dilution with cleaner scrap [4]. Using chlorination followed by oxidation processes to separate copper from steel is proposed in different studies. Although the authors stated that the process is technically feasible, large production amounts in the steel industry restrain using chlorine gas due to environmental and safety issues [7, 8]. The alloying effect on Cu bearing steels is studied to minimize the hazardous impact of Cu. Manganese, sulphur, silicon, phosphorus, and nickel effect on Cu in steel are studied from different researches [9–14]. The effect of Cu and Sn on the oxidation mechanism of steel is studied by Konda [15, 16] with a low amount of Sn and Cu. Studies have shown those tramp elements have a vital role in the oxidation of steel besides detrimental effects on mechanical properties. Our previous studies have shown that Cu affects mill scale characteristics of hot rolled steel slabs [17]. In this study, oxidation kinetics of low and high copper containing steel samples are studied. Oxidation kinetics and surface morphology with

✉ Selçuk Yeşiltepe, yesiltepes@itu.edu.tr; Mustafa Kelami Şeşen, mksesen@itu.edu.tr | [1]Metallurgical and Materials Engineering Department, Istanbul Technical University, Istanbul, Turkey.

scale characterizations are applied to understand Cu effect on the oxidation kinetics of steel.

2 Experimental

Samples for oxidation kinetics were prepared via machining of steel castings with different amounts of copper. Samples were produced in an induction furnace by smelting. 0.20% Cu sample was casted then copper alloyed to liquid steel. Carbon was decreased in 2.00% sample, alloying time caused decarburization and copper diluted the carbon amount. Chemical compositions of the samples were given in Table 1. Samples are prepared as rectangular shape measure of $20 \times 20 \times 5$ mm. Surface areas of the machined samples were calculated manually and the samples were placed in alumina crucibles. They were put in a pre-heated electric resistance furnace. The furnace was adjusted to the ambient conditions during the experimental procedure. Experiments were carried out for 10, 20, 30, 60, and 90 min at the oxidation temperatures between 900 and 1200 °C with 100 °C intervals. Mass gain of the samples were carried out from the mass difference of oxidized and initial samples in Precisa™ XB320M sensitive balance. The oxidation rate was calculated as the mass gain per surface area. Kinetical values were evaluated with the Arrhenius equation, and the calculation procedure is obtained from the previous study [18]. X-ray diffraction (XRD) investigations of the scales were carried out using a Panalytical™ X'Pert Pro with Cu Kα (k = 1.5406 Å) radiation in the 2θ range of 20–70 at a rate of 2/min. The surfaces of the samples were grinded up to 2500 mesh using SiC papers followed by polishing with 1 µ alumina paste. Then polished samples were washed with distilled water and ethanol. Dried samples were etched with a solution of 10 g of $FeCl_3$–10 ml H_2O_2–100 ml distilled water. The surfaces of the samples were examined with optical microscopy via Olympus X70 microscope. Then they were examined with SEM imaging and EDS analysis for detailed investigations. Initial microstructures of the samples were given in Fig. 1. Initial microstructures did not contain any copper segregation. Microstructures of the materials consisted dendritical grains of typical casting structure.

3 Results and discussion

The results of the oxidation rate were given in Fig. 2. Oxidation rate increased according to the oxidation temperature and exposure time. Cu bearing steel had the same oxidation behavior with low Cu steel at 900 °C. Oxidation level of the steel increased due to the temperature as expected. Higher temperature increased the mass gain of copper-bearing steel more than mass gain of the low copper steel. The oxidation rate of steel with high copper content showed an increasing trend with time. Longer

Table 1 Chemical composition of oxidized steel samples

Sample	C%	Mn%	Si%	S%	P%	Cr%	Cu%	Ni%
0.20% Cu	0.419	0.45	0.39	0.02	0.017	0.1	0.2	0.09
2.00% Cu	0.209	0.47	0.48	0.02	0.017	0.1	1.96	0.09

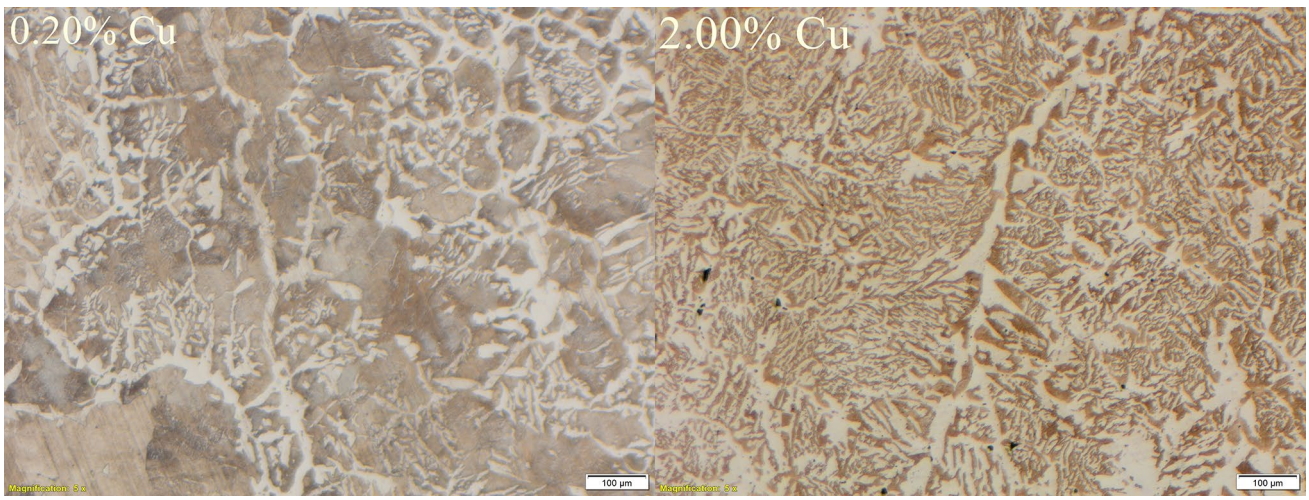

Fig. 1 Original microstructure of samples (0.20% Cu on left, 2.00% Cu on right)

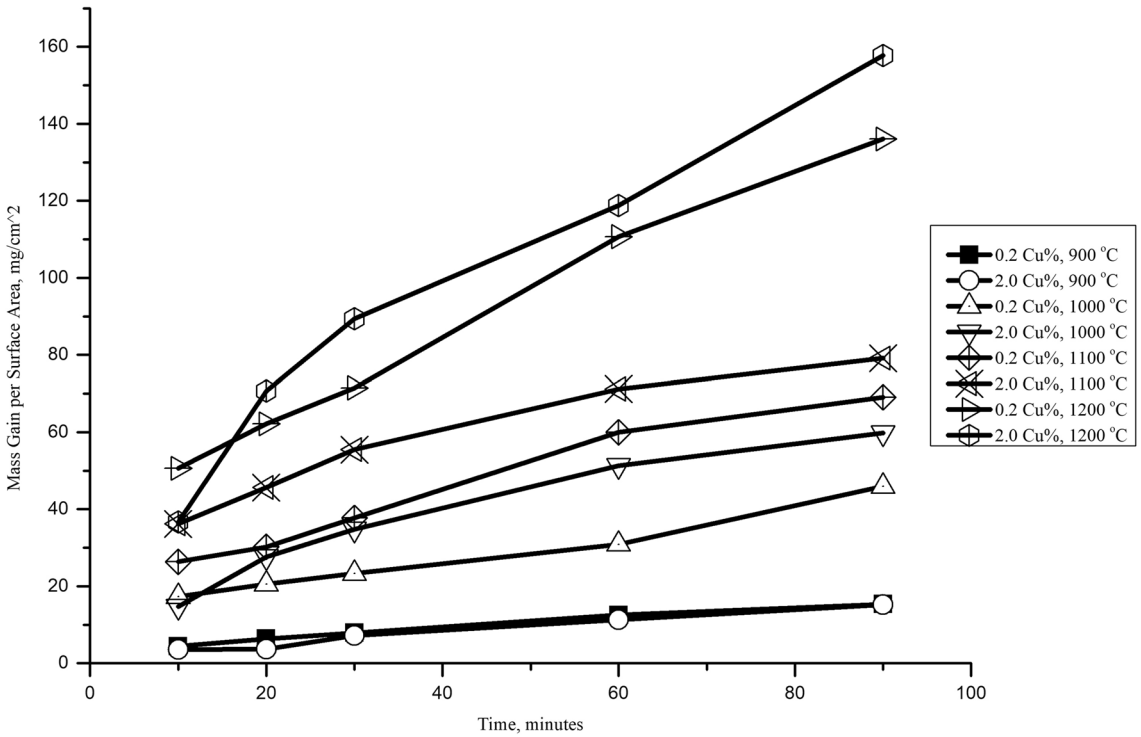

Fig. 2 Oxidation rate of 0.20% Cu and 2.00% steel for 900, 1000, 1100 and 1200 °C

exposing time to the oxidative atmosphere broke the oxidation resistance of steel with copper alloying. Exposing the material to the shorter oxidation durations revealed a protective mechanism against oxidation. The oxidation resistance of material decreased due to the time of exposure. After 30 min of oxidation, all specimens had a stable oxidation regime.

XRD results for scales of oxidized samples were given in Fig. 3. Figure 3 showed that increasing copper content in steel increased the oxidation rate. Higher oxygen-containing phases of iron such as hematite formed in scale in 2.00% Cu containing steels. Wustite phase was mainly eliminated in 2.00% Cu containing steel. Magnetite exists in both scales due to thermodynamics because wustite is the most stable phase of iron oxide at elevated temperatures. This result explained higher mass gain in copper-containing steel due to the formation of hematite. The formation of hematite also declared the oxidation process of the surface was completed. The completion of oxidation on the steel surface mean the kinetical model of oxidation was controlled by diffusion. Further oxidation of iron atoms below the surface needs ion exchange from the iron oxides on the surface. That situation decreased the oxidation rate of the steel after 30 min.

SEM and EDS analysis showed copper enrichment under the mill scale, as stated in the literature for hot shortness mechanism [19]. The copper-rich region was found in 2.00% Cu containing steel. SEM images, along with optical microscopy images, showed copper segregation on the steel surface. The optical microscopy image of 0.20% Cu is given in Fig. 4, and the image of 2.00% Cu image is provided in Fig. 5. Optical and SEM images showed a cross-sectional view of the steel surface. Figure 4 showed resin mold, scale, decarburization zone, and original microstructure from top to bottom. All images were collected with the same structure. SEM images of 2.00% Cu bearing steel after oxidation treatment with EDS analysis were given in Figs. 6, 7 and 8. EDS analysis of samples was presented in Tables 2 and 3, respectively.

EDS results of Fig. 5 showed copper segregation under the scale. Blister formation under the scale was visible from the SEM image. EDS analysis showed copper segregation along with sulfur content. The thermodynamic point of view states sulphur affinity of copper is higher than iron [20]. Inner oxide particles could be seen below the surface and copper segregation. Blister formation due to vapour pressure of liquid copper and CO that formed during the decarburization of the surface decreases steel-scale cohesion. Previous study revealed that blister formation also related with Kirkendall effect caused by segregated phases diffusion constant [21]. Figure 6 and EDS analysis showed a smoother oxidation surface without large blisters. Inner oxide formation was less than Fig. 5. It was reported that fayalite formation possible in silicon and silicon-copper

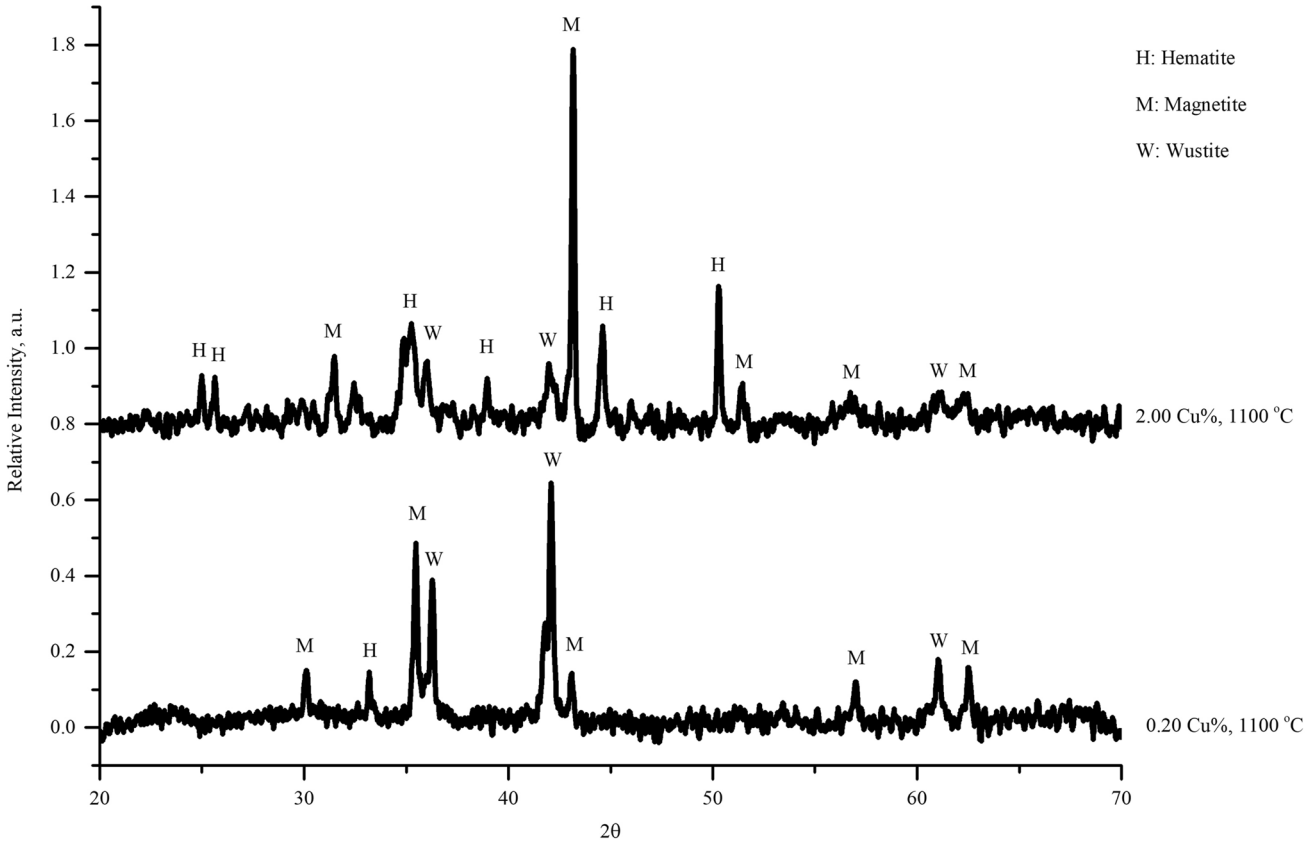

Fig. 3 XRD results of scales of 0.20% and 2.00% Cu containing steels at 1100 °C

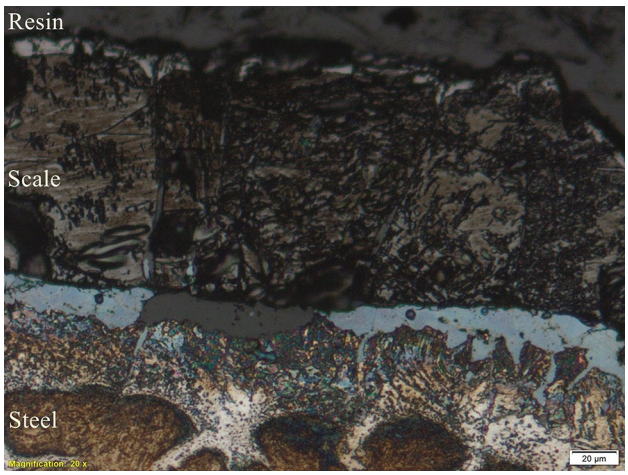

Fig. 4 The cross-sectional view of the optical microscope image of 0.20% Cu bearing steel after oxidation at 1100 °C for 90 min

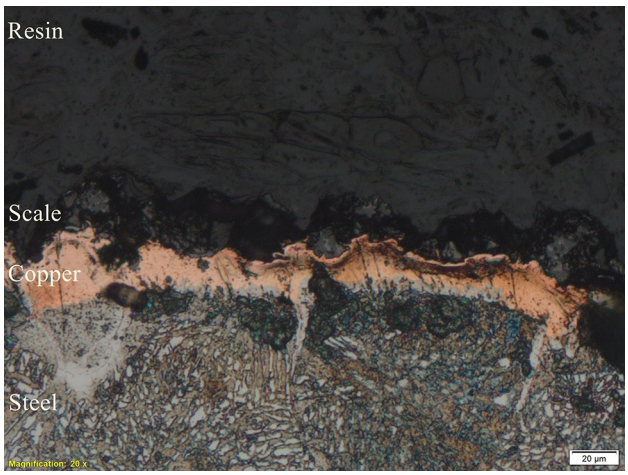

Fig. 5 The cross-sectional view of the optical microscope image of 2.00% Cu bearing steel after oxidation at 1100 °C for 90 min

containing steels but fayalite formation restricted due to surface decarburization [22, 23]. Copper segregation below the surface could be seen with the penetrated copper on the steel grain boundaries. Segregated copper on the surface followed the path of austenite grain boundaries and diffused to the inner parts of the steel. Similar behaviour of copper was reported by previous research [22].

Kinetical model was derived from the study of Cao et al. [18] that based on the Arrhenius equation. Mass gain per

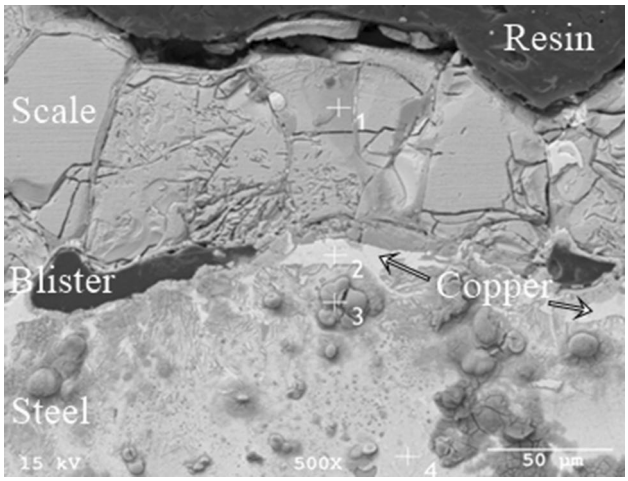

Fig. 6 The cross-sectional view of the SEM image of 2.00% Cu bearing steel after oxidation at 1100 °C for 90 min

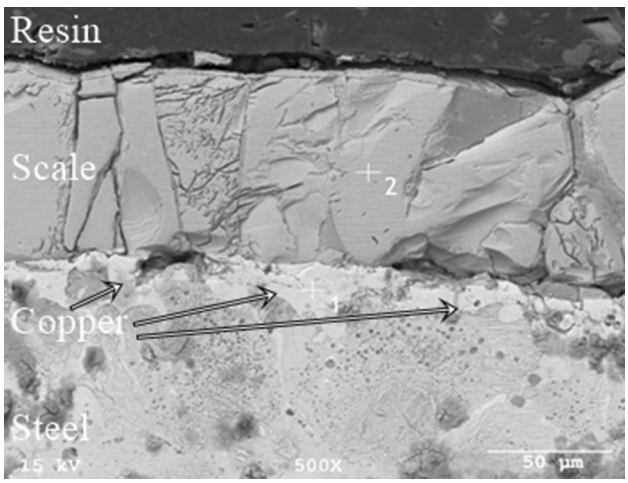

Fig. 7 The cross-sectional view of the SEM image of 2.00% Cu bearing steel after oxidation at 1100 °C for 90 min

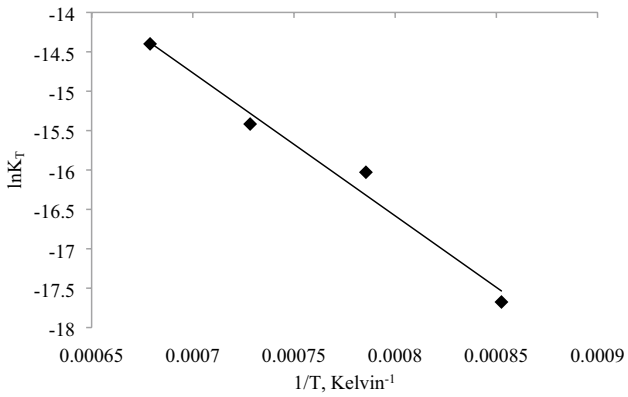

Fig. 8 ln K_T–1/T relationship for 0.20% Cu Alloy

Table 2 Point EDS analysis results of Fig. 5

Spot	Fe%	Cu%	Mn%	O%	S%
1	67.98	–	6.598	25.42	–
2	15.37	57.12	–	–	27.51
3	89.51	2.63	–	7.86	–

Table 3 Point EDS analysis results of Fig. 6

Spot	Fe%	Cu%	O%
1	13.3	86.7	–
2	86.92	–	13.08

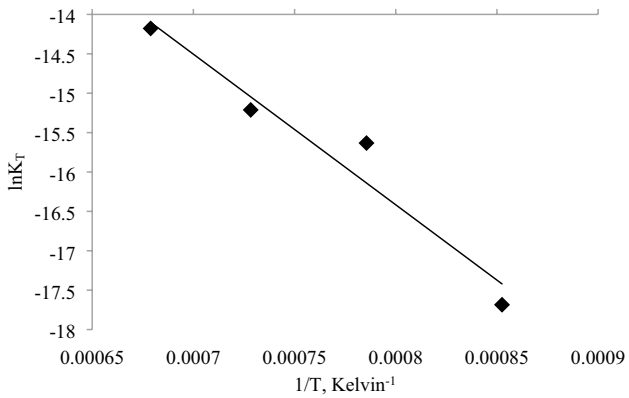

Fig. 9 ln K_T–1/T relationship for 2.00% Cu Alloy

area was used for the determination of the oxidation rate constant of the oxidation process. Oxidation rate constant was calculated by using the equation:

$$\Delta W^n = K_T \cdot t$$

where ΔW is the mass gain of material per surface area, K_T is oxidation rate constant, and t is time. The mass gain of material can be expressed in mg mm^{-2} and time in minutes. n is a constant that proposed for different scale types. In loose and porous scale structures n is $n < 2$ for compact scales $n > 2$ [18]. In this study, n value was set to 1.5 because of blister formation on the scale. Blister formation decreased compactness of the scale. Calculations were based on this formulae, and activation energy was calculated from the slope of ln K_t–T^{-1} line. ln K_t–T^{-1} graphic was plotted in Figs. 7 and 8 for 0.20% Cu alloy and Fig. 9 for 2.00% Cu alloy consecutively. T is the temperature in Kelvins. Calculated K_t values for 90-min oxidation were given in Table 4.

The calculated activation energy of oxidation for 0.20% Cu and 2.00% Cu alloys were 150.9 kJ/mol and 159.1 kJ/mol, respectively. The activation energy for the oxidation

Table 4 Calculated K_t values for 90 minutes of oxidation

Sample	K_t ($mg^2\ mm^{-4}\ min^{-1}$)
0.20% Cu, 900 °C	2.106×10^{-8}
0.20% Cu, 1000 °C	1.094×10^{-7}
0.20% Cu, 1100 °C	2.017×10^{-7}
0.20% Cu, 1200 °C	5.578×10^{-7}
2.00% Cu, 900 °C	2.087×10^{-8}
2.00% Cu, 1000 °C	1.625×10^{-7}
2.00% Cu, 1100 °C	2.474×10^{-7}
2.00% Cu, 1200 °C	6.961×10^{-7}

Table 5 Activation energy of oxidation in different steel compositions

Steel	Activation energy (kJ/mol)	Atmosphere	Source
Low Si-steel	150.48	20% H_2O/Ar	[12]
High Si-steel	181.25	20% H_2O/Ar	[12]
Low C steel	125.50	21% O_2–79% N_2	[18]
0.06% Sn low–C steel	142.07	O_2	[24]
Low-C steel	164.80	20% O_2/Ar	[25]
0.20% Cu low–C steel	150.90	Air	This study
2.00% Cu low–C steel	159.10	Air	This study

of steel was calculated for various compositions under different atmospheric conditions. The comparisons of the activation energies of the previous investigations were given in Table 5. Generally, low carbon steels have activation energies of oxidation between 125 and 180 kJ/mol. The activation energies for Cu bearing carbon steels were in the range of 125–180 kJ/mol value. The copper effect on oxidation activation energies in steel were insignificant but the oxidation process was affected dramatically. Blister formation in scale–steel interface is unique for copper-bearing steels.

Formation of liquid segregated copper layer between steel–scale interface decreased the steel–scale cohesion. Decreased cohesion between the steel and scale, along with vapour pressure from molten copper, creates a free surface for blister formation. Liquefied copper acts as a protective layer in the early stages of the oxidation. Steel with lower copper content had an adherent scale on the surface. Adherent scale formation created a smooth pathway of diffusion for further oxidation. The formation of segregated copper on the steel surface created a blockage for oxygen diffusion. Lower oxygen affinity of copper restrained oxidation of copper in the presence of iron. Hematite formation in high copper-bearing steel was the result of a disconnected scale from the steel surface by segregated copper. Restrained oxygen diffusion to steel was given in Fig. 10.

Kinetical phenomenon proposes two different pathways; chemical controlled and diffusion controlled. Oxidation of copper-bearing steel occurs in two steps; chemical controlled process occurs at the beginning of oxidation, the high oxidation rate is observed in this step, diffusion-controlled mechanism takes place after the formation of scale on the steel surface with a stable oxidation rate. In the diffusion-controlled stage of oxidation, copper-bearing steel has two protective mechanisms: loose scale and liquid copper segregation on the surface. Copper bearing steel needs higher activation energy for oxidation because of restrained oxygen diffusion to the steel surface. The difference between high and low copper bearing steel derives from the segregation of copper on the steel surface. The general oxidation mechanism of copper-bearing steel is illustrated in Fig. 11. The scale on the steel surface forms after short exposure time to the oxidative atmosphere at elevated temperatures. Liquid copper particles

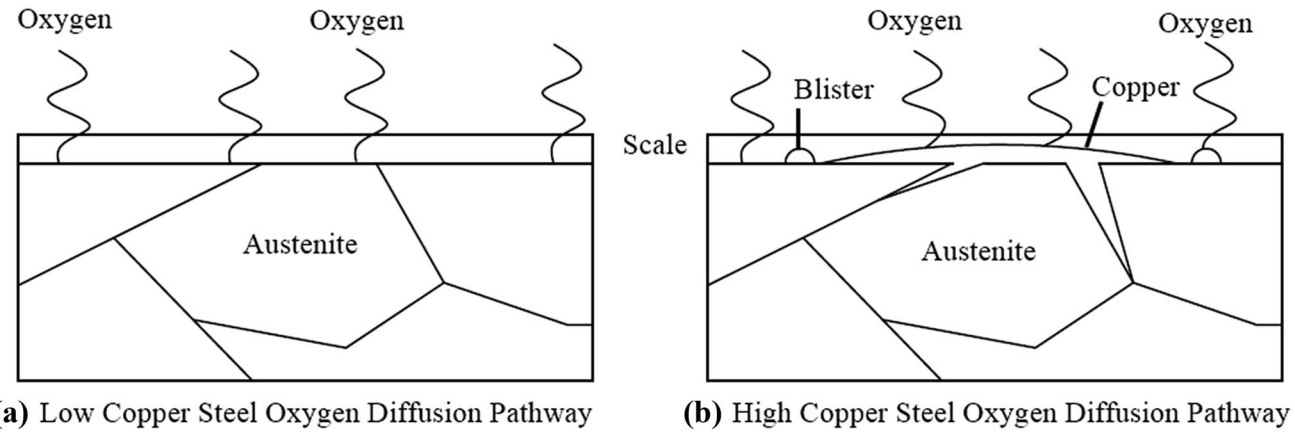

Fig. 10 Oxygen diffusion pathways in low copper and high copper bearing steels

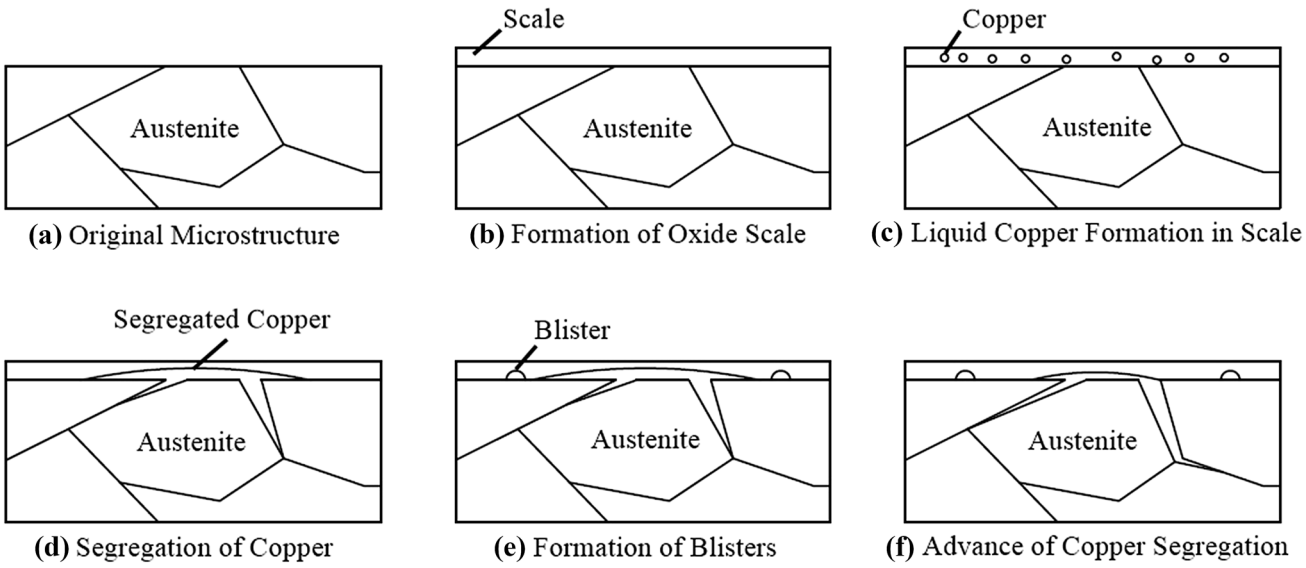

Fig. 11 Illustration of oxidation mechanism in copper bearing steel

form in scale in case of higher oxidation temperatures than coppers melting point, 1083 °C. Copper particles accumulate on the steel surface to decrease formation energy. Liquid copper film penetrates the material through grain boundaries. Vapour pressure from molten copper, along with the CO discharge from decarburization, creates blisters on the steel surface. Liquid copper advances to inner parts of material by following the grain boundaries and causes intergranular cracks on the steel surface.

4 Conclusion

Results showed that copper segregates at elevated temperatures, and it works as an oxygen barrier on the steel surface. This mechanism results in increased activation energy of oxidation in copper-bearing carbon steel.

(1) The copper amount is found to be ineffective at 900 °C for the oxidation rate of steel; however, at elevated temperatures, copper enhances the mass gain rate of steel. Higher copper content increases the oxidation level of steel. Hematite is found in 2.00% Cu containing steel scale, while 0.20% Cu containing steel scale consists of magnetite and wustite.
(2) The formation of blisters on the scale/metal interface restrains the diffusion of oxygen atoms to the inner parts of the material. Liquid copper existence under scale also suppresses the diffusion pathway of oxygen atoms. This mechanism works as a protective surface condition on the steel surface and results in elevated activation energy of oxidation in copper-bearing steel. Copper bearing steel has an activation energy of oxidation 159.10 kJ/mol, while low copper bearing steel has 150.90 kJ/mol activation energy.
(3) Cu has higher oxidation resistance than iron, thus remains in the metallic form under the steel surface and causes segregates on the steel surface. Segregated copper migrates to austenite grain boundaries and decreases grain cohesion. This mechanism, along with high temperature and rolling process results in macro cracks known as hot shortness.

Compliance with ethical standards

Conflict of interest The authors declare that they have no competing interests.

References

1. Björkman B, Samuelsson C (2014) Recycling of steel. In: Worrell E, Reuter M (eds) Handbook of recycling: state-of-the-art for practitioners, analysts, and scientists. Elsevier, Amsterdam, pp 65–83. https://doi.org/10.1016/B978-0-12-396459-5.00006-4
2. Nakamura S, Kondo Y, Matsubae K et al (2012) Quality- and dilution losses in the recycling of ferrous materials from end-of-life passenger cars: input–output analysis under explicit consideration of scrap quality. Environ Sci Technol 46:9266–9273. https://doi.org/10.1021/es3013529
3. Nakajima K, Yamasue E, Ishihara KN et al (2014) Total material requirement of scrap steel from end-of-life vehicle. Tetsu-to-Hagane 100:778–787. https://doi.org/10.2355/tetsutohagane.100.778

4. Daehn KE, Cabrera Serrenho A, Allwood JM (2017) How will copper contamination constrain future global steel recycling? Environ Sci Technol 51:6599–6606. https://doi.org/10.1021/acs.est.7b00997
5. Kuzuhara S, Sakuma H, Hayashi H, Daigo I (2017) Spatial distribution of tramp element contents in recycled steel. ISIJ Int 57:758–763. https://doi.org/10.2355/isijinternational.isijint-2016-508
6. Rod O, Becker C, Nylén M (2006) Opportunities and dangers of using residual elements in steels: a literature survey. Jernknotoret Rep 88042:1–59
7. Shin SM, Lee DW, Ha SA, Wang JP (2013) Study of cyclic oxidation for copper removal from solid ferrous scrap in end-of-life vehicle (ELV). Adv Mater Res 699:869–874. https://doi.org/10.4028/www.scientific.net/amr.699.869
8. Tee JKS, Fray DJ (2006) Separation of copper from steel. Ironmak Steelmak 33:19–23. https://doi.org/10.1179/174328106x80028
9. Urata K, Kobayashi Y (2016) Precipitation mechanism of copper sulfides in solid iron. J Jpn Soc Exp Mech 16:342–347
10. Ono-Nakazato H, Taguchi K, Kawauchi D, Usui T (2006) Separation of Fe and Sn–Cu phases in an Fe–Sn–Cu–B system Sn-rich. Mater Trans 47:864–867
11. Uchino H, Nagasaki C, Kaga M, Seo S-J, Asakura K, Shibata K (2001) Effects scrap of C and P on surface hot shortness of steel due to Cu mixed from steel amount of steel scrap. J Adv Sci 13:260–264
12. Webler BA, Sridhar S (2007) The effect of silicon on the high temperature oxidation behavior of low-carbon steels containing the residual elements copper and nickel. ISIJ Int 47:1245–1254. https://doi.org/10.2355/isijinternational.47.1245
13. Comineli O (2014) A novel concept of high Cu, low Mn, environmentally-friendly weathering steels. Mater Sci Forum 783–786:698–703. https://doi.org/10.4028/www.scientific.net/msf.783-786.698
14. Imai N, Komatsubara N, Kunishige K (2008) Effects of Cu and other tramp elements on steel properties. effect of Cu and Ni on hot workability of hot-rolled mild steel. ISIJ Int 37:224–231. https://doi.org/10.2355/isijinternational.37.224
15. Kondo Y (2008) Behaviour of copper during high temperature oxidation of steel containing copper. ISIJ Int 44:1576–1580. https://doi.org/10.2355/isijinternational.44.1576
16. Kondo Y (2007) Effect of atmospheric conditions on copper behaviour during high temperature oxidation of a steel containing copper. ISIJ Int 47:1309–1314. https://doi.org/10.2355/isijinternational.47.1309
17. Yeşiltepe S, Şeşen MK (2019) In: Mladenovic S, Maluckov C (eds) 51th International October Conference, in Bor, Serbia, pp 118–122
18. Cao G, Liu X, Sun B, Liu Z (2014) Morphology of oxide scale and oxidation kinetics of low carbon steel. J Iron Steel Res 21:335–341. https://doi.org/10.1016/S1006-706X(14)60051-0
19. Shibata K, Seo S-J, Kaga M et al (2002) Environmentally benign manufacturing and material processing toward dematerialization. suppression of surface hot shortness due to Cu in recycled steels. Mater Trans 43:292–300. https://doi.org/10.2320/matertrans.43.292
20. Cha W-Y, Kobayashi Y, Susa M et al (2015) Growth rate of copper sulfide precipitates in solid low carbon steel. ISIJ Int 55:103–108. https://doi.org/10.2355/isijinternational.55.103
21. Gong YF, De Cooman BC (2010) Kirkendall void formation during selective oxidation. Metall Mater Trans A Phys Metall Mater Sci 41:2180–2183. https://doi.org/10.1007/s11661-010-0356-6
22. Chen RY, Yuen WYD (2005) Copper enrichment behaviours of copper-containing steels in simulated thin-slab casting processes. ISIJ Int 45:807–816. https://doi.org/10.2355/isijinternational.45.807
23. Fukagawa T, Okada H, Maehara Y (1994) Mechanism of red scale defect formation in Si-added hot-rolled steel sheets. ISIJ Int 34:906–911. https://doi.org/10.2355/isijinternational.34.906
24. Chandra-ambhorn S, Jutilarptavorn A, Rojhirunsakool T (2019) High temperature oxidation of irons without and with 0.06 wt% Sn in dry and humidified oxygen. Corros Sci 148:355–365. https://doi.org/10.1016/j.corsci.2018.12.030
25. Ha SA, Kim DK, Lee WJ et al (2014) Comparison study of oxidation behavior of low carbon steel at elevated temperatures. Adv Mater Res 1025–1026:504–508. https://doi.org/10.4028/www.scientific.net/AMR.1025-1026.504